

# **Amino acid-based polymeric hydrogel and nanoparticles for neuroregeneration and siRNA-drug loaded formulation for anticancer applications**

A Dissertation

Submitted in partial fulfilment of the requirement for the

**Degree of Philosophy**

by

**Ms. Kirti Wasnik**

(Roll No.: 17021507)

**Supervisor:**

**Dr. Pradip Paik**

(Associate Professor)



School of Biomedical Engineering  
Indian Institute of Technology (Banaras Hindu University)  
Uttar Pradesh  
Varanasi 221 005, India

**March, 2024**

## Declaration by the Candidate

I, **Ms. Kirti Wasnik**, Ph.D. Scholar (Roll no. 17021507), certify that the work embodied in this Dissertation: "**Amino acid-based polymeric hydrogel and nanoparticles for neuroregeneration and siRNA-drug loaded formulation for anticancer applications**". is my own bonafide work that carried out by me under the supervision of **DR. PRADIP PAIK**, School of Biomedical Engineering, Indian Institute of Technology, BHU, Varanasi, India, from "**2017**" to "**2024**", at the School of Biomedical Engineering, Indian Institute of Technology (BHU), Varanasi, India.

I declare that I have faithfully acknowledged the research works and have been cited them whichever have been followed to carry out the work of this Dissertation.

This dissertation is free from plagiarism and has not been submitted previously in part or in full to this or any other University or Institution for the award of any degree or diploma.

Place: IIT BHU

Date: 5<sup>th</sup> March, 2024



(Ms. Kirti Wasnik)

## CERTIFICATE BY the SUPERVISOR

It is certified that the above statement made by the student is true to the best our knowledge.



(Supervisor)

Dr. Pradip Paik,  
Associate Professor,  
School of Biomedical Engineering,  
Indian Institute of Technology, BHU, Varanasi, India

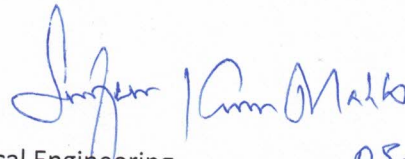
05/03/2024

सह-आचार्य/ASSOCIATE PROFESSOR  
जैव चिकित्सा अभियांत्रिकी स्कूल  
SCHOOL OF BIOMEDICAL ENGG  
भारतीय प्रौद्योगिकी संस्थान (का.हि.वि.)  
INDIAN INSTITUTE OF TECHNOLOGY (B.H.U.)  
वाराणसी-221005/VARANASI-221005

(COORDINATOR)

School of Biomedical Engineering,  
Indian Institute of Technology, BHU, Varanasi, India  
समन्वयक/CO-ORDINATOR

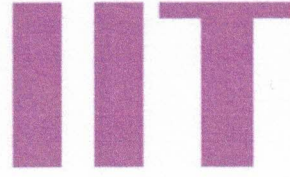
जैव चिकित्सा अभियांत्रिकी स्कूल  
SCHOOL OF BIOMEDICAL ENGG.  
भारतीय प्रौद्योगिकी संस्थान (का.हि.वि.)  
INDIAN INSTITUTE OF TECHNOLOGY (B.H.U.)  
वाराणसी-221005/VARANASI-221005



05.03.2024



भारतीय  
प्रौद्योगिकी  
संस्थान  
काशी हिन्दू विश्वविद्यालय



INDIAN  
INSTITUTE OF  
TECHNOLOGY  
BANARAS HINDU UNIVERSITY

**Dr. Pradip Paik**, B.Tech. (C.U), M.Tech. & Ph.D. (IIT-K)  
Associate Professor  
School of Bio-Medical Engineering

Varanasi, U.P., India  
Phone.: +91-8500109932(m)  
Fax: +91-.-  
Email: paik.bme@iitbhu.ac.in,  
pradip.paik@gmail.com

Ref:

Paik/IIT(BHU)/1

Date: 5<sup>th</sup> March, 2024

### CERTIFICATE

This is to certify that **Ms. Kirti Wasnik**, Research Scholar (Roll no. **17021507**), performed Ph.D. dissertation under my supervision at the School of Biomedical Engineering, Indian Institute of Technology (IIT), Banaras Hindu University (BHU). The dissertation entitled: "**Amino acid-based polymeric hydrogel and nanoparticles for neuroregeneration and siRNA-drug loaded formulation for anticancer applications**" is a Bonafide record of research work carried out by her under my supervision and guidance. This dissertation work has not been submitted previously in part or full to any other Institute or University for the award of any Degree or Diploma. This dissertation is free from plagiarism (report attached)

It is also certified that the student has fulfilled all the requirements to submit this dissertation.

Further, parts of this dissertation have been filed for patents or published in peer-reviewed journals to fulfil the requirement of the Degree and all rights reserve to the IIT (BHU), Varanasi, India.

**Dr. Pradip Paik**,  
Associate Professor,  
School of Biomedical Engineering,  
Indian Institute of Technology, BHU  
Varanasi

सह-आचार्य/ASSOCIATE PROFESSOR  
जैव चिकित्सा अभियांत्रिकी स्कूल  
SCHOOL OF BIOMEDICAL ENGO.  
भारतीय प्रौद्योगिकी संस्थान (का.हि.वि.)  
INDIAN INSTITUTE OF TECHNOLOGY (B.H.U.)  
वाराणसी-221005/VARANASI-221005



SCHOOL OF BIOMEDICAL ENGINEERING  
INDIAN INSTITUTE OF TECHNOLOGY (BHU)  
✉ paik.bme@iitbhu.ac.in, pradip.paik@gmail.com  
🌐 http://www.iitbhu.ac.in/bme



Regd. No. 2123/GO/Re/S/21/CPCSEA

Date: 03 May, 2022

IAEC Approval Number: **IIT(BHU)/IAEC/2022/079**

**CERTIFICATE**

This is to certify that the project proposal entitled “**siRNA and Drugs (Taxol, DOX, Temozolomide, curcumin, Mangiferin, MTX, immunomodulatory drugs etc.) loaded novel bio-polymeric Nano-formulation for Biomedical Applications such as (a) Neuron Regeneration and (b) Anticancer activity against multidrug resistance cancer using Rat and mice model**” submitted by **Ms. Kirti Wasnik** under supervision of **Dr. Pradeep Paik** has been approved/recommended by the IAEC of *Indian Institute of Technology, Banaras Hindu University, Varanasi* in its meeting dated **03/05/2022** and has been sanctioned **25 Female Wistar Rats (200-250 gm), 34 Female BALBc Mice (20-25 gm)** under this proposal for a duration of **Twelve (12) months.**

Prof. Sushant Kumar  
Shrivastava  
**Name & Signature**

**Chairman**

Dr. Vinod Tiwari  
**Name & Signature**

**Member Secretary**

Dr. Shesh Narayan Mishra  
**Name & Signature**

**Main Nominee of CPCSEA**

***Note: The CPCSEA Guideline should be followed strictly while handling the animals***

## **COPYRIGHT TRANSFER CERTIFICATE**

**Title of the Thesis:** Amino acid-based polymeric hydrogel and nanoparticles for neuroregeneration and siRNA-drug loaded formulation for anticancer applications

**Name of the Student:** Kirti Deepak Wasnik

### **Copyright Transfer**

The undersigned hereby assigns to the Indian Institute of Technology (BHU), Varanasi all rights under copyright that may exist in and for the above thesis submitted for the award of the Doctor of Philosophy.



**Date:** 05<sup>th</sup> March 2024

**Place:** Varanasi

**Signature of the Student**  
(Kirti Wasnik)

**Note:** However, the author may reproduce or authorize others to reproduce material extracted verbatim from the thesis or derivative of the thesis for author's personal use provided that the source and the Institute's copyright notice are indicated.



---

# Dedicated

*To my beloved parents,  
Brothers, sister-in-law,  
and friends.*

---



## *ACKNOWLEDGEMENTS*

---

It is my greatest pleasure to have this opportunity to express my sincere appreciation to everyone who helped me during my Ph.D. program at the Indian Institute of Technology (Banaras Hindu University), Varanasi. First, I would like to express my deepest gratitude to my supervisor Dr. Pradip Paik, for his valuable guidance, encouragement and his paternal behaviour throughout the work. His inspiring and excellent guidance is the key reason that I could successfully finish each of the research objectives.

I would like to express my appreciation to my research progress evaluation committee (RPEC) members, Dr. Sanjeev K. Mahto and Dr. Ashutosh Dubey, for their kind cooperation during the course of this work. I am also grateful to Prof. Pralay Maiti, School of Materials Science and Technology, Prof. Shantanu Das Ceramic Engineering and Dr. Sudip Mukherjee for helping me with valuable guidance and encouragement.

I would like to extend my sincere thanks to faculty members of the School of Biomedical Engineering, IIT(BHU) Prof. Prasun K. Roy, Prof. Neeraj Sharma, Dr. Shiru Sharma, Dr. Sanjay Kumar Rai, Dr. Marshal, Dr. Jac Fredo, Dr. Deepesh Kumar, Dr. Brijesh Kumar and Dr. Gauri Balachandran.

I would like to extend my sincere thanks to Prof. Arbind Acharya and Dr. Richa Arya, Assistant Professor, Department of Zoology, BHU.

I would like to thanks Prof. Rajeev Prakash, In-Charge, Central Instrument Facility Centre and his team members for providing all the characterization facilities on time with precision, without which the completion of this work was not possible. I also wish to express thankfulness to all other respected faculty members of the School for their kind support and valuable suggestions.

I would like to thank Thanks to seniors, especially Dr. Munendar Sing Tomar, Dr. Somdutta, Dr. Ravi Prakash, Dr. Meenakshi, Dr. Alok Prakash, Dr. Nilima Varshney, Dr. Ajay Sahi. And my friends Mrs. Bindu Kumari, Mr. Prem Shankar Gupta, Mr. Divakar, Mr. Vipin Rai, Mr. Sandeep, Mrs. Hrashda, Mr. Subhansu, Mr. Rakesh, Mr. Manas Gupta, Mrs. Manisha, Mrs. Anshi, Ms. Papri , Ms. Swikriti and Ms. Sudipta.

I would like to thank my wonderful lab-mates Gurmeet Singh, Desh Deepak Yadav, Divya Pareek, Sukanya Patra, Prem Shankar Gupta, for their stimulating discussions and creating a cheerful environment in the lab. I would also like to thank my batch-mates and friends Pratik Purohit, Shravanya, Dr. Sumit, Nill Mani, Prem, Sneha, Pankaj and all my juniors for their extended support. I thank all my beloved friends across the globe for sharing my happy and sorrow moments at all times.

I would like to sincerely thank to all the supporting staff of the School for their kind help whenever I required.

I can never forget my parents Mr. Deepak Wasnik, Late. Babarao Deshmukh, Ushabai Deshmukh and Mrs. Durga Wasnik and Siblings Aniket, Kapil, Rupali Sweety whose boundless love, constant inspiration, emotional support and blessings has provided me encouragement at every step of life. My parents' everlasting shower of blessing kept me moving easily with all hazards vanishing miraculously.

Lastly, I would like to thank Almighty, for having made everything possible by giving me strength and courage to do this work.

# Table of Contents

---

CHAPTER. 1; INTRODUCTION AND LITERATURE REVIEW		1-51
1.1.	INTRODUCTION	1
1.2.	LITERATURE REVIEW	5
1.2.1.	Polymer And Hydrogel:	5
1.2.1.1.	Poly (Amino Acid) And Synthesis Strategies' For Amino Acid Based Functional Polymer.	5
1.2.1.2.	Applications Of Polymer Depend On Its Physical, Chemical, And Other Properties	7
1.2.1.3.	Amino Acid Based Polymers And Their Biomedical Applications	10
1.2.2.	Advantages Of Computational Methodologies For Biomedical Applications	12
1.2.3.	Neuron Regenerative Approaches	13
1.2.3.1.	Global Statistic Of Neuro Degeneration And Cerebral Cancer	14
1.2.3.2.	Vulnerability Of Adult Neuron For Degeneration	16
1.2.3.3.	Role Of Angiogenesis In Neuron Growth And Neurotherapy	17
1.2.3.4.	Current Status Polymer Used In Neuron Repair And Growth	18
1.2.4.	Basic Information On Cancer	20
1.2.4.1.	Global Statistics Of Cancer	21
1.2.4.2.	Genetic Alteration And Global Challenge In Treatment Of Aggressive Cancer.	22
1.2.4.3.	Amino Acid Transporters And The Therapeutic Target In Cancer.	23
1.2.4.4.	Role Of Polymers In Cancer Treatment	24
1.2.4.5.	Role Of Sirna For Cancer Treatment	25
1.2.4.6.	Sirna Mediated RNA Interference Mechanism	25
1.2.4.7.	Chemically Modified Sirna And Its Advantages As Therapeutics.	26
1.2.4.8.	Sirna And Drugs In Cancer Treatment	28
1.2.4.9.	Advantages Of Sirna/ Drug For Co-Delivery	29

1.2.4.10.	Challenges In Sirna Designing And Anticancer Therapy.	31
1.3.	RESEARCH GAP AND MOTIVATION	32
1.4.	MAJOR OBJECTIVES.	33
CHAPTER: 2 MATERIALS, METHODS, AND CHARACTERIZATION		
TECHNIQUES		52-64
2.1	. INTRODUCTION.	52
2.2.	MATERIALS AND METHODS	52
2.2.2	Synthesis of N-acryloyl glycine and N-acryloylglutamate monomers	52
2.2.3	Preparation Of Poly(N-Acryloylglycine-Acrylamide) Co-Polymeric Hydrogel.	53
2.2.4.	Synthesis Of P(NAG-Ac-NAE) Nanohydrogel.	54
2.2.5.	Characterization Of NAG, P(NAG-B-A) And P(NAG-Ac-NAE) Co-Polymeric Hydrogel.	54
2.2.6.	Morphological Evaluation. Morphology And 3D Structural Analysis Of P(NAG-B-A) Co-Polymeric Hydrogel	55
2.2.7.	Swelling Behavior Of Poly(NAG-B-A) Co-Polymeric Hydrogel And P(NAG-Ac-NAE) Hydrogel.:	55
2.2.8.	Rheological Behavior Of Hydrogel.	56
2.2.9.	In Vitro Cytotoxicity Assay.	57
2.2.10.	Animal Ethics Permission.	57
2.2.11.	Cortical Neuron Isolation And Primary Culture.	57
2.2.12.	Immunofluorescence Staining.	58
2.2.13.	Hemocompatibility Of Hydrogel.	59
2.2.14.	In-Vitro Recovery From Oxidative Stress.	59
2.2.15.	Determination Of Intracellular ROS Generation And Effect On Mitochondrial Potential.	60
2.2.16.	Egg Yolk Angiogenesis Assay.	61
2.2.17.	Wound Scratch Assay.	61
2.2.18.	Live And Dead Assay.	62
2.2.19	Apoptosis And Necrotic Assay.	62
2.2.20.	Semi-quantitative reverse transcription and polymerase chain reaction (sqRT-PCR)	63

2.2.21	Statistical Analysis.	63
2.2.22.	Protein Ligand Interaction Screening.	63
2.2.23.	Theoretical and computational methodology..	64
CHAPTER 3: Results And Discussion (Part-I)		65-110
3.1.1.	Abstract	65
3.1.2	Introduction	66
3.1.3.	EXPERIMENTAL	70
3.1.4.	RESULTS	74
3.1.4.1	Synthesis:	72
3.1.4.2	Physical And Physicochemical Properties Of Hydrogel.	76
3.1.4.3	Morphology Of P(NAG-B-A) Co-Polymeric Hydrogel.	78
3.1.3.5	Rheological Properties Of P(NAG-B-A) Hydrogel.	82
3.1.3.6	Biocompatible P(NAG-B-A) Hydrogel Protects Cytoskeletal Framework Of Cortical Neurons.	84
3.1.3.7	Study The P(NAG-B-A) Hydrogel Assisted Neurogenesis.	86
3.1.4.4	Molecular Interaction Between Polymer And GSK3 $\beta$ .	91
3.1.3.8	Protective Role Of P(NAG-B-A) In Oxidative Stress	95
3.1.3.9	Discussion	98
CHAPTER 3: Results And Discussion (Part-II)		111-158
3.2.1	Objective I:	111
3.2.3	EXPERIMENTAL	115
RESULTS		
3.2.4.1	Physical Characteristics of p(NAG-Ac-NAE) Hydrogel.	119
3.2.4.2	Swelling Behavior of p(NAG-Ac-NAE) Hydrogel.	122
3.2.4.3	Biodegradation Behaviours.	124
3.2.4.4	Viscoelastic and Rheological flow behaviour	126
3.2.4.5	Cytocompatibility and Hemocompatibility of p(NAG-Ac-NAE)	127
3.2.4.6	p(NAG-Ac-NAE) hydrogel induced primary neurite outgrowth.	130
3.2.4.7	Neuroprotective role of p(NAG-Ac-NAE) hydrogel.	132
3.2.4.8	Comparative ROS Mitigating Effect of p(NAG-Ac-NAE) and p(NAG-b-Ac) Hydrogel.	135

3.2.4.9	Angiogenesis stimulatory effect of p(NAG-Ac-NAE) hydrogel.	138
3.2.4.10	Effect of Hydrogel on Gene Expression Analysis.	141
	DISCUSSION.	144
	CHAPTER 3. RESULTS AND DISCUSSION (PART-III)	159-198
3.3.1	ABSTRACT.	159
3.3.2	INTRODUCTION.	160
3.3.3	Methodology	163
3.3.4	RESULTS	168
3.3.4.1	Theoretical bioactivity assessment of p(NAG-b-A).	168
3.3.4.2	DFT Calculation of randomized structure of p(NAG-b-A) polymeric unit.	168
3.3.4.4	Comparative heparanase inhibitory activity of p(NAG-b-A) polymeric units: molecular docking based investigation.	171
3.3.4.5	Swelling index and biodegradation investigation of p(NAG-b-A).	178
3.3.4.6	p(NAG-b-A) hydrogel enhances the cytotoxicity in aggressive cancer: a comparative assessment.	179
3.3.4.7	p(NAG-b-A) hydrogel selectively mitigate the cancer cell migration	183
3.3.4.8	p(NAG-b-A) hydrogel elevated the Reactive Oxygen Species (ROS) for apoptotic cell death	187
3.3.4.9	Heparanase inhibitory activity.	189
3.3.5	Discussion	190
	CHAPTER 3: Results And Discussion (Part-IV)	199-229
3.4.1	Abstract	199
3.4.2	Introduction	200
3.4.3	Methodology	204
3.4.4	Results And Discussion	210
3.4.4.1	Physical characterization.	210
3.4.4.2	Morphology of p(NAPA-co-LME) NPs	211
3.4.4.3	Thermal stability of particles.	214

3.4.4.4	Heparanase inhibitory activity of the particles	217
3.4.4.5	siPOLR2A encapsulation and serum stability of p(NAPA-co-LME)-co-siPOLR2A complex.	218
3.4.4.6	Cell Viability of p(NAPA-co-LME) NPs and p(NAPA-co-LME)-co-siPOLR2A complex	219
3.4.4.7	Cellular uptake and Internalization mechanism of p(NAPA-co-LME) NPs and p(NAPA-co-LME)-co-siPOLR2A complex.	222
3.4.4.8	CHAPTER: 4 SUMMARY, CONCLUSIONS And FUTURE SCOPES	230-238
	Appendix-1:	239-249
	Appendix-2	250-257
	Appendix-3	258-
	CHAPTER 3: Results And Discussion (Part-III)	266

## LIST OF FIGURES

---

Figure 1.1. 1 Synthetic strategies of various amino acid functional polymer [14]	7
Figure 1.1. 2 Age-standardised DALY rates ranking for different neurological disorders reported by GBD(Year 2015)	15
Figure 1.1. 3 Various neurological disorders in 2015	15
Figure 1.1. 4 Schematic of TNBC heterogeneity showing TNBC subtype's main histopathology, markers, and signaling pathways [164]	21
Figure 1.1. 5. siRNA mediated RNA interference mechanism. (a) Structural orientation of siRNA which composed of 19 nucleotide with overhang structure. (b) Argounote 2 protein and its structural domains (c) siRNA or miRNA mediated silencing mechanism where siRNA loaded with TRBP and AGO2 protein and form the active RISC complex, which eventually degrade the mRNA and inhibit the translation	27
Scheme3.1. 1 Shows the probable mechanism involved in the synthesis of poly(N-acryloylglycine-acrylamide) hydrogel.	75
Scheme3.1. 2 Synthesis of poly(N-acryloylglycine-acrylamide) co-polymeric hydrogel and various processing steps to achieve its different forms.	78
Figure 3.1. 1 Morphology and particle size distribution analysis of p(NAG-b-A) co-polymeric hydrogel. (a)-(b) SEM micrographs, (c-d) HRTEM micrographs, (e) histogram for average particle size distribution obtained from (c) and (d), and (f) the pore size distribution obtained from HRTEM images (Figure 3.1.d).	80
Figure 3.1. 3. Swelling behavior of p(NAG-b-A) co-polymeric hydrogel. (a) Pictorial representation of swelling behavior of hydrogel at different pH of PBS, (b) percentage of mass swelling index at different pH and (c) volume swelling index of hydrogel at different pH.	82
Figure 3.1. 4 Rheological properties of p(NAG-b-A) co-polymeric hydrogel were studied with different conditions. Frequency ( $\omega$ ) sweep measurements of p(NAG-b-A) hydrogel were performed at different temperatures (34 °C, 37 °C, 40 °C and	84

---

43 °C); (a) storage modulus vs.  $\omega$ ; (b) loss modulus vs.  $\omega$ , at different temperature; and (c) complex viscosity ( $\eta^*$ ) vs.  $\omega$  at different temperatures. (d) Viscosity ( $\eta$ ) flow behavior of p(NAG-b-A) hydrogel as a function of shear rate ( $\dot{\gamma}$ ); (e) Viscosity ( $\eta$ ) as a function of time and temperature and (f) show the change in shear stress with shear rate at different temperatures.

---

Figure 3.1. 5. Cytocompatibility and neurotoxicity results of p(NAG-b-A) co-polymeric hydrogel. (a) Show the cell viability results on HEK293, HepG2, and PC12 cells at different concentrations of p(NAG-b-A) hydrogel. (b) Shows the primary neuron differentiation in control and with different concentrations of hydrogel (50, 100 and 500  $\mu\text{g mL}^{-1}$ ). (c) Acridine orange and PI staining of PC12 cells grown on the control and p(NAG-b-a) hydrogel of concentration 100  $\mu\text{g mL}^{-1}$  and 500  $\mu\text{g mL}^{-1}$  concentration on 5th day. 87

---

Figure 3.1. 6 Confocal microscopy images represent the neuronal growth on p(NAG-b-A) co-polymeric hydrogel: 500  $\mu\text{g mL}^{-1}$  granular nanohydrogel coated slide (p(NAG-b-A), A-group), p(NAG-b-A) hydrogel film (p(NAG-b-A), B-group) and control (poly(L-lysine) coated slide) till the 14th day. (a) Cellular adhesion and growth on 2nd day, (b) cellular differentiation and neurite extension on 7th day and (c) cellular differentiation and neurite extension on 14th day, (d) cellular proliferation (%) obtained from images. (e) Shows how the longest axonal path varied at different time periods, and (f) shows the increase in number of junctions (branching in neurons) at different time periods. Hoechst 33258 (blue) stains represent the nucleus, immune labeled b-Tubulin III (green) shows neurite extension and immune labeled with phalloidin (red) showed the F-actin (all the Confocal microscopy images captured in 20X). 90

---

Figure 3.1. 7 Molecular interactions between GSK3 $\beta$  (PDBID-1Q5K) with reference inhibitors. (a) Surface structure shows the ATP binding pockets with TMU inhibitor, (b) ribbon conformation of 1Q5K with N-(4-methoxybenzyl)-N'-(5-nitro-1,3-thiazol-2-yl) urea (TMU) and ligplot shows the interacted residues, (c) ribbon conformation of 1Q5K-SB415286 and ligplot shows the interacted residues with two different pockets and (d) ribbon conformation of 1Q5K-SB216763 and ligplot shows the interacted residues of amino acid with highest binding energy in kcal mol $^{-1}$  and  $K_i$  (inhibition constant). 93

---

Figure 3.1. 8. Molecular interactions between GSK3 $\beta$  (PDBID-1Q5K) with different monomeric di-units (a-d) and tri-units ((e)-(h)) of poly (N-acryloylglycine-acrylamide). N-acryloylglycine represented as (G) and N-acrylamide represented as (A), (a) 1Q5K- N-acryloylglycine, (b) 1Q5K-GG (N-acryloylglycine di-unit), (c) 1Q5K-GA (N-acryloylglycine-acrylamide di-unit), (d) 1Q5K-AA (acrylamide di-unit), (e) 1Q5K-GGG (homomeric tri-unit of N-acryloylglycine), (f) 1Q5K-AGG (tri-unit of N-acryloylglycine and N-acrylamide), (g) 1Q5K-GAG (tri-unit of N-acryloylglycine and N-acrylamide), and (h) 1Q5K-AAG (triunit of N-acryloylglycine and acrylamide). Ribbon structure shows the docking site between 1Q5K and ligplot with each structure showing the interacted residue along with binding energy in kcal mol<sup>-1</sup> and inhibition constants (K<sub>i</sub>) in mM or  $\mu$ M or pM.

---

Figure 3.1. 9 Protective role and recovery status after H<sub>2</sub>O<sub>2</sub> induce oxidative stress associated damage assisted by p(NAG-b-A) hydrogel. (a) Protective role of p(NAG-b-A) hydrogel obtained by cell viability assay, (b) stress induced recovery status of PC12 cells using p(NAG-Ac-NAE) hydrogel, (c) Raman shifting of p(NAG-Ac-NAE) hydrogel, (d) AO/EtBr staining of PC12 cells untreated control, treated with H<sub>2</sub>O<sub>2</sub> (40  $\mu$ M), and treated with 40  $\mu$ M H<sub>2</sub>O<sub>2</sub> along with 500  $\mu$ g mL<sup>-1</sup> of p(NAG-b-A) hydrogel and (e) cytoskeleton network stabilization by p(NAG-b-A) hydrogel in the presence of 40  $\mu$ M H<sub>2</sub>O<sub>2</sub> induced oxidative stress at highest proliferative concentration of 500  $\mu$ g mL<sup>-1</sup> hydrogel.

---

Figure 3.2. 1 Physical properties of poly-[(N-acryloyl-glycine)-co-(acrylamide)-co-(N-acryloyl glutamate)] (p(NAG-Ac-NAE)) hydrogel. (a) FESEM micrograph, (b) and (c) HRTEM micrograph at low and high magnification, respectively. (d) SAED pattern of the particles. (e) and (f) Average particle size distribution obtained from Figure 3.2.1(a) and (b) respectively. (g) Pore size distribution of the particles obtained from 1c, and (h) XRD pattern of nanohydrogel.

---

*Scheme 3.2. 1 Representative steps of synthesis of poly-[(N-acryloylglycine)-co-(acrylamide)-co-(N-acryloylglutamate)] co-polymeric hydrogel*

---

Figure 3.2. 2 . Swelling and degradation behavior (a) MSI of the hydrogel at different pH of PBS, (b) Degradation of hydrogel in different pH, (b) MSI of hydrogel in different enzymes and (c) Degradation of hydrogel in the presence of

---

different enzymatic solutions: Lysozyme, Proteinase K and collagenase IV with 100  $\mu\text{g mL}^{-1}$  concentration and PBS.

---

Figure 3.2. 3 (a-f) Rheological properties were measured at different temperatures, 126  
34 °C, 37 °C, 40 °C and 43 °C; (a) storage modulus vs. angular frequency, (b) loss  
modulus vs. angular frequency, and (c) complex viscosity ( $\eta^*$ ) vs. angular  
frequency. (d) Change in shear stress vs. Shear rate at different temperatures, (e)  
viscosity ( $\eta$ ) flow behavior of p(NAG-Ac-NAE) hydrogel as a function of shear  
rate ( $\dot{\gamma}$ ) and (f) viscosity ( $\eta$ ) as a function of time and temperature.

---

Figure 3.2. 4 cytocompatibility and hemocompatibility of poly(NAG-Ac-NAE) 129  
co-polymeric hydrogel. (a) cell viability in HUVEC, PC12 and of cancer cell line  
LN229, MDA-MB-231 and MCF7 in presence of p(NAG-Ac-NAE) hydrogel. (b)  
Live/Dead (AO/PI stained) macroscopic images PC12 cells in treatment of  
p(NAG-Ac-NAE) hydrogel at concentration of 100  $\mu\text{g mL}^{-1}$  and 250  $\mu\text{g mL}^{-1}$  on  
day 5, (c) % hemolysis at different concentrations hydrogel (1000, 500, 250, 125  
and 62.5  $\mu\text{g mL}^{-1}$ ) (d) Microscopy images of primary neuronal cells in treatment  
of p(NAG-Ac-NAE) hydrogel (50 and 100  $\mu\text{g mL}^{-1}$ ), and (e) cytoskeleton  
framework of primary neuron in presence of p(NAG-Ac-NAE) hydrogel of  
concentration 100  $\mu\text{g mL}^{-1}$  and 250  $\mu\text{g mL}^{-1}$ , (red-F-actin and blue- nucleus)  
only

---

Figure 3.2. 5. Confocal microscopy images of neuron growth on 250  $\mu\text{g mL}^{-1}$  131  
nanohydrogel coated slide and a thin slice of poly(NAG-Ac-NAE) co-polymeric  
hydrogel. (a) Nature of cellular adhesion and growth on day 2nd. (b) Cellular  
differentiation and neurite extension on day 7th and (c) and (d) cellular  
differentiation and neurite extension on day 14th and day 21st, respectively on  
control, p(NAG-Ac-NAE) coated slide (250  $\mu\text{g mL}^{-1}$ ) and sliced p(NAG-Ac-  
NAE) polymeric hydrogel. (e) Estimated increase in cell population at different  
intervals of culture (f) longest axonal path varied at different periods and (g)  
increased number of junctions (branching in neuron) changed at different periods.  
Hoechst 33258 (blue) stain represents the nucleus, immune-labelled  $\beta$ -tubulin III  
(green) shows neurite extension, and immune labelled with phalloidin (red) shows  
the F-actin.

---

Figure 3.2. 6 Neuroprotective role of p(NAG-Ac-NAE) hydrogel. 133

(a) Protective role of p(NAG-Ac-NAE) hydrogel in presence of different concentrations of H<sub>2</sub>O<sub>2</sub>, (c-d) stress-induced recovery status of PC12 cells using p(NAG-Ac-NAE)hydrogel after H<sub>2</sub>O<sub>2</sub> – induce stress, (e) Fluorescent microscopy images for the AO/EtBr stained PC12 cells at different conditions: untreated control, treated with H<sub>2</sub>O<sub>2</sub> 40  $\mu$ M mL<sup>-1</sup> and H<sub>2</sub>O<sub>2</sub> 20  $\mu$ M mL<sup>-1</sup> in p(NAG-Ac-NAE) hydrogel in H<sub>2</sub>O<sub>2</sub> 40  $\mu$ M.mL<sup>-1</sup>, p(NAG-Ac-NAE) hydrogel in H<sub>2</sub>O<sub>2</sub> 20  $\mu$ M mL<sup>-1</sup> and (f) cytoskeleton network stabilization by p(NAG-Ac-NAE) hydrogel and in the presence of 40  $\mu$ M mL<sup>-1</sup> H<sub>2</sub>O<sub>2</sub> induced OS at highest proliferative concentration of 250  $\mu$ g mL<sup>-1</sup> hydrogel, respectively which further confirmed by cell cycle analysis.

---

Figure 3.2. 7 Stress mitigating effect analysis through cell cycle analysis. DNA content detected by flow cytometry in treatment of p(NAG-b-Ac), p(NAG-Ac-NAE), H<sub>2</sub>O<sub>2</sub>, H<sub>2</sub>O<sub>2</sub> along with p(NAG-b-Ac) and H<sub>2</sub>O<sub>2</sub> along p(NAG-Ac-NAE) hydrogel. 134

---

Figure 3.2. 8 Represents the effect of p(NAG-Ac-NAE) hydrogel and p(NAG-b-Ac) hydrogel on mitochondrial membrane potential and on intracellular ROS production in PC12 cells. (a) reduction of mitochondrial membrane potential depolarization observed in H<sub>2</sub>O<sub>2</sub> oxidative stress by p(NAG-Ac-NAE)hydrogel and p(NAG-b-Ac) hydrogel, (b) Flow cytometry detection of intracellular ROS in PC12 cells: (b1) untreated control, ( b2) exposure of H<sub>2</sub>O<sub>2</sub> 20  $\mu$ M (b3) exposure of H<sub>2</sub>O<sub>2</sub> 40  $\mu$ M, (b4) treatment with p(NAG-Ac-NAE)hydrogel, ( b5) exposure of H<sub>2</sub>O<sub>2</sub> 20  $\mu$ M treatment with p(NAG-Ac-NAE)hydrogel, (b6) exposure of H<sub>2</sub>O<sub>2</sub> 40  $\mu$ M treatment with p(NAG-Ac-NAE)hydrogel, (b7) treatment with p(NAG-b-Ac) hydrogel, (b8) exposure of H<sub>2</sub>O<sub>2</sub> 20  $\mu$ M and treatment with p(NAG-b-Ac) hydrogel and (b9) exposure of H<sub>2</sub>O<sub>2</sub> 40  $\mu$ M and treatment with p(NAG-b-Ac) hydrogel. (c) FTIR spectrum of (c1 and c2) H<sub>2</sub>O<sub>2</sub> treated and without treated p(NAG-Ac-NAE) hydrogel, (b) H<sub>2</sub>O<sub>2</sub> without treated and treated p(NAG-b-Ac) hydrogel, and (c) Raman spectrum at different treatment conditions. 137

---

Figure 3.2. 9 Angiogenic stimulatory effect of p(NAG-Ac-NAE) hydrogel. (a) In ovo CEA assay in the presence of p(NAG-Ac-NAE) enhanced the vascular sprouting (marked as a black arrow) in dose dependent manner. (b-e) show the change in several angiogenic parameters, such as blood vessel area, the total 140

---

number of junctions, junctions density and total vessel length obtained in time-dependent (statistical significance level of  $*p < 0.05$ ).

Figure 3.2. 10 Figure 3.2.10. Figure 3.2.9 (a) Change in HIF 1 $\alpha$ , VEGF and KDR mRNA expression in treatment of p(NAG-b-A) and p(NAG-Ac-NAE) in presence and in absence of H <sub>2</sub> O <sub>2</sub> induce oxidative stress at 20 $\mu$ M and 40 $\mu$ M concentrations against PC12 cells. After sqRT-PCR, the amplicon was separated on 2% agarose gel. Densitometry analysis were performed using FIJI software represented in graph. Figure (b). Change in VEGFa, IL1- $\beta$ , and TNFa mRNA expression in treatment of p(NAG-b-A) and p(NAG-Ac-NAE) at 25 and 250 $\mu$ g mL <sup>-1</sup> in RAW264.7 cells. After sqRT-PCR, the amplicon was separated on 2% agarose gel. Densitometry analysis was performed using FIJI software and represented in graphs.	143
Figure 3.3. 1 Theoretical bioactivity scores of random arrangements of N-acryloyl glycine, acrylamide and cross linked structures categorized into: (1) linear homopolymer (G1 to G11), (2) linear hetopolymer (GA series), (3) cross-linked homopolymer (D1 to D6), and (4) cross-linked hetopolymer (D7 to D25). Series 1: protease inhibitor, Series 2: GPCR ligand, Series 3: Ion channel modulator, Series 4: Kinase inhibitor, Series 5: Nuclear receptor ligand, and Series 6- enzyme inhibitor.	169
Figure 3.3. 2 Ground state HOMO, and excited state LUMO and energy band gap of (a) homopolymer of n-acryloyl glycine, (b) Linear hetro-polymer of N-acryloylglycine and acrylamide and (c) cross-linked monomeric to hexameric unit of p(NAG-co-Ac) polymer. (d) Molecular orbital of glycine in HOMO to LUMO energy transfer, (e) molecular orbital of N-acryloyl glycine in HOMO to LUMO energy transfer, and (f) D4 and D22, D6 and D7	172
Figure 3.3. 3 3D protein structure of heparanase (7PRT) depicting the catalytic domains and heparin binding domains HBDI, HBDII and HBIII. Docking poses a complex of (b) Cyclophellitol, and (c) Roneparstat with 7PRT.	175
Figure 3.3. 4 Docking poses for complex of (i) Glycine, (ii) N-acryloylglycine, (iii) G2, (iv) GA1, (v) AA, (vi)GA4, (vii)D2 and (viii) D24 with 7PRT	176

Figure 3.3. 5 Docking poses for complex for (ix) D4, (x) D21, (xi) D22, (xii) D18, (xiii) G6, (xiv) GA17, (xv) D5 and (xvi) D20 with 7PRT	177
Figure 3.3. 6 Morphology, mass swelling ratio and degradation behavior of poly-[(N-acryloylglycine)-co-(acrylamide)] hydrogel in different enzymatic solutions. (a) FESEM micrograph of p(NAG-co-Ac), (b) particle size distribution obtained from Figure 3.3.1(a). (c) Mass swelling ratio of p(NAG-co-Ac) in PBS and different enzymatic solution lysozyme, proteinase K and collagenase I at the concentration 100 $\mu\text{g mL}^{-1}$ of enzyme, (d-i) FESEM micrograph of degraded p(NAG-co-Ac) at 15th day and particle size distribution using respective micrograph (d-e) p(NAG-co-Ac) in PBS, (f-g). p(NAG-co-Ac) in 100 $\mu\text{g mL}^{-1}$ lysozyme, (h-i) p(NAG-co-Ac) in 100 $\mu\text{g mL}^{-1}$ proteinase K.	178
Figure 3.3. 7 MTT assay represents the cell viability results on (a) L929 (b) HEK 293 (c) HepG2 (d) MCF7 (e) A549 (f) MDA-MB-231 and (g) LN229 cell lines treated with different concentrations of glycine (red), N-acryloyl glycine (blue) and p(NAG-co-Ac) hydrogel (green)	181
Figure 3.3. 8 (a) Live and dead assay studied via AO/PI staining of MDA-MB-231 cell lines treated with glycine, N-acryloylglycine and p(NAG-co-Ac) hydrogel, and (b) hemolysis percentage in treatment with p(NAG-co-Ac) hydrogel	182
Figure 3.3. 9 The in vitro wound scratch assay results obtained using LN229 glioblastoma cells by applying different concentrations (50 $\mu\text{g mL}^{-1}$ , 100 $\mu\text{g mL}^{-1}$ and 250 $\mu\text{g mL}^{-1}$ ) of samples. Results obtained for (a) glycine, (b) N-acryloyl glycine, (c) p(NAG-co-Ac) and (d) migration. The inhibition was measured in terms of wound closer percentage observed at 24 and 48 hrs	184
Figure 3.3. 10 The in-vitro wound scratch assay using MDA-MB-231 triple negative breast cancer cell line (TNBC) by applying different concentrations (50 $\mu\text{g mL}^{-1}$ , 100 $\mu\text{g mL}^{-1}$ and 250 $\mu\text{g mL}^{-1}$ ) of (a) glycine, (b) N-acryloylglycine, (c) p(NAG-co-Ac) and (d) migration. The inhibition was measured in terms of wound closer percentage observed at 24 and 48 hours.	183
Figure 3.3. 11(a) Flow cytometry based quantitative analysis (using Annexin V/PI assay) of apoptotic and necrotic cell death induced by glycine, N-acryloylglycine and p(NAG-co-Ac) hydrogel and compared to the untreated reference control. (b-e) Intracellular ROS generation induced by (b) glycine at 50 and 500 $\mu\text{g mL}^{-1}$ , (c) N-acryloylglycine 50 and 500 $\mu\text{g mL}^{-1}$ , (d) p(NAG-co-Ac) hydrogel 50 and 500	187

$\mu\text{g mL}^{-1}$ , and (e) comparison of intracellular ROS generation between Figure 3.3.11 b, c, and d.

Figure 3.3. 12 Comparison of anti-antigenic effect of N-acryloylglycine and p(NAG-co-Ac) hydrogel. (a) In ovo CEA assay, in the presence of p(NAG-co-Ac) restricted the vascular sprouting (marked as black arrow) in dose dependent manner compared to N-acryloyl glycine. The change in vessel area, total number of junctions, junction density, total vessel length and average vessel length changed with dosing of: (b-f) N-acryloylglycine and (g-k) dosing of p(NAG-co-Ac) hydrogel as shown in time dependent manner with statistical significance level of $p < 0.05$ .	190
Figure 3.3. 13 Heparanase inhibitory activity of glycine, n-acryloyl and p(NAG-b-Ac)	191
Figure 3.4. 1 FTIR spectra of (a) N-acryloyl phenylalanine methyl ester monomer, (b) N-acryloyl leucine methyl ester monomer, (c) poly (N-acryloyl phenylalanine methyl ester) NPs (p(NAPA)NP), poly(N-acryloyl Leucine methyl ester) NP p(LME), and poly[(N-acryloyl phenylalanine methyl ester)-co-(N-acryloyl Leucine methyl ester)] NP (p(NAPA-co-LEM)NP).(d) UV-Vis spectra of p(LME), p(NAPA) and p(NAPA-co-LEM) NPs.	212
Figure 3.4. 2(c) MALDI-ToF spectra of p(NAPA-co-LEM)NPs	213
Figure 3.4. 3 Morphological characteristics of (a-e) p(NAPA), (f-j) p(LME) and (k-o) p(NAPA-co-LEM)NP. Figure (a, f and k) represent low magnification TEM macrographs. Figures (b,g and l) represent HRTEM macrographs of respective polymeric nanoparticles. Figures (c, h and m) represent the XRD of particles with SAED pattern obtain from HRTEM of respective polymer. Figures (d, i and n) show the particle size distribution of nanoparticles obtained from HRTEM micrographs and Figures (e, j and o) represent the pore size distribution of the obtained particles.	215
Figure 3.4. 4 Zeta potential of (a) p(NAPA), (b) p(LME) and (d) p(NAPA-co-LEM) NPs	216

Figure 3.4. 5 Thermogravimetric analysis (TGA) and Differential Scanning Calorimetry (DSC) of (a-b) p(NAPA), (c-d) p(LME) and (e-f) p(NAPA-co-LME) NPs	217
Figure 3.4. 6 Comparative Heparanase inhibitory activity of p(NAPA), p(LME) and p(NAPA-co-LME) NPs.	218
Figure 3.4. 7 siRNA encapsulation and serum stability. Figs. (a-c) represent the siRNA encapsulation in p(NAPA), p(LME) and p(NAPA-co-LME) NPs, where ‘M’ represent 100 bp ladder, ‘S’ represents the naked duplex siRNA, ps, ls, and pls- represent supernatant siRNA of different concentration of 20 $\mu$ M ( $\approx$ 200ng) siRNA, 10 $\mu$ M ( $\approx$ 100ng) siRNA and 5 $\mu$ M ( $\approx$ 50ng) siRNA with respective type of nanoparticle; es, el and pl- represent the encapsulated siRNA in p(NAPA)NP, p(NALE) NP and p(NAPA-co-NALE) NP, lane 4, 5, 6 of each gel of a, b and c represent supernatant obtained after siRNA encapsulation and lane 7, 8 and 9 represent encapsulated particle. Figs. d-g represent the serum stability: (d) naked duplex siPOR2A, (e) naked 5-base-assymetric-Cy3-siPOLR2A, (f) p(NAPA-co-LME)-co-siPOLR2A and (g) p(NAPA-co-LME)-co-(5b(A)Cy3-siPOLR2A) complex at different time interval lane 1-100bp ladder, lane 2-7 different time interval 0, 3, 6, 12, 24 and 48 h.	220
Figure 3.4. 8 Cell Viability of p(NAPA-co-LME) NPs and p(NAPA-co-LME)-co-siPOLR2A complex: (a) treatment with different concentrations of p(NAPA-co-LME) particles to normal cell line PC12, HepG2 and L929 and cell viability (b) cytotoxicity of cancer cell in response to p(NAPA-co-LME) particles, (c) MDA-MB 231 cell viability in response to paclitaxel(PTX) and p(NAPA-co-LME) +PTX NPs, (d) MDA-MB-231 cell viability in response to the siPOLR2A (loaded and naked siRNA) and (e) MDA-MB-231 cell viability in response to different combinations of siRNA: Drug and co-loaded particles.	223
Figure 3.4. 9 Western blot of POLR2A (217 kDa) (a) silencing with 5b(A)Cy3-siPOLR2A and (b) silencing with duplex siPOLR2A	224
Figure 3.4. 10 Cellular Internalization mechanism and endolysosomal escape. Fig (a-f): show flow cytometry based cellular uptake of NP, Fig (c), cellular uptake in response to the different inhibitors, (d) chloropramazin, (e) amilroid and (f) Nystatin. Figs. (g-h) confocal microscopic	225

images of LAT1 mediated internalization of P(NAPA-co-LME)-5b(A)Cy3-siPOLR2A at 2 hours and 6 hours. (I and J) endolysosomal escape.

S3.1. 1 FTIR Spectrum of N-acryloylglycine (NAG) monomer.	239
S3.1. 2 <sup>1</sup> H NMR and <sup>13</sup> C NMR (a) <sup>1</sup> H NMR of N-acryloylglycine monomer and (b) <sup>13</sup> C NMR of N-acryloylglycine monomer. Fig. S2(a) shows the <sup>1</sup> H NMR (DMSO-d <sub>6</sub> ) spectrum of NAG with the corresponding chemical shifts (δ in ppm): 12.5 (O—H of carboxylic acid), 8.4 (N—H of 2° amine), 6.1(=C—H <sub>2</sub> ), 6.3 (cis) and 5.6 (trans) of (H <sub>2</sub> C=CH <sub>2</sub> ), 3.4 for H <sub>2</sub> O and 2.5 for DMSO-d <sub>6</sub> . <sup>13</sup> C-NMR (Fig. S3.1.2(b)) spectrum confirmed the presence of 5 carbon moiety with the corresponding chemical shift at 175 ppm (—COOH), 165 ppm (O=C—NH-R), 125 ppm (—HC-NH), 132 ppm (C=C) and 40 ppm band of DMSO-d <sub>6</sub> .	240
S3.1. 3. FTIR Spectrum of poly(N-acryloylglycine-acrylamide) co-polymeric hydrogel.	241
S3.1. 4. (a) <sup>1</sup> H NMR of p(NAG-b-A) hydrogel and (b) <sup>13</sup> C NMR of p(NAG-b-A)nanohydrogel.	242
S3.1. 5(a). Solubility test of the p(NAG-b-A) hydrogel in different solvents at room temperature.	243
S3.1. 6. Thermal stability and heat flow shown in Fig.(a) represents TGA of p(NAG-b-A) co-polymeric hydrogel and Fig. (b) represents DSC plot of p(NAG-b-A) hydrogel.	244
S3.1. 7. (a) XRD pattern of NAG and (b) XRD pattern of p(NAG-b-A).	245
S3.1. 8. (a) Size distribution of p(NAG-b-A) hydrogel NPs and (b) zeta potential (ζ) of p(NAG-b-A) hydrogel in water measured through DLS at room temperature.	245
S3.1. 9. Show the actin filament stabilization in primary neuron cultured on Fig. (a) poly (l) lysine coated slide (control) and on Fig. (b) p(NAG-b-A) hydrogel. All fluorescent microscopy images were acquired at 10X and cells were stained with the Hoechst 33258 and immunolabeled with Phalloidin. Images show the merged (Hoechst 33258 + F-actin) and bright field (merged) images.	246

S3.1. 10. Figure shows the 3D orientation of the longer neurite growth on the 2D substrate (Figs. a-f) (for A-group). Figs (g-l) show the neurite growth in longer and deep penetration depth of p(NAG-b-A) hydrogel on 14th Day of culture (B-group sample). Figs. (a) and (g) are for Hoechst 33258 staining of nucleus of neurons, Figs. (b) and (h) for the beta tubulin III immunolabeled hippocampal neurons, Fig. (c) and (i) Phalloidin (red) immunolabeled hippocampal neuron; Figs. (d) and (j) represent the merged images of immunolabeled hippocampal neurons; Figs. (e) and (k) show the bright field images of hippocampal neurons and Figs. (f) and (l) show the merged 3D images of bright field and immunolabeled stained neurons, respectively.	247
S3.1. 11 FTIR and Raman shift of untreated and H2O2 treated p(NAG-b-A) hydrogel	248
S3.2 1. (a) FTIR spectra of N-acryloylglycine, (b) N-acryloylglutamic acid, (c) poly [(N-acryloylglycine)-b-(acrylamide)] (d) poly(N-acryloylglycine)-co-(acrylamide)-co-(N-acryloylglutamate) co-polymeric hydrogel.	251
S3.2 2. (A) 1H NMR of N-acryloylglutamate monomer and (B) 13C NMR of N-acryloylglycine monomer	252
S3.2 3. (A) 1H NMR of p(NAG-Ac-NAE) nanohydrogel and (B) 13C NMR of p(NAG-Ac-NAE)) nanohydrogel.	253
S3.2 4. (a) TGA and (b) DSC of the poly(N-acryloylglycine)-co-(acrylamide)-co-(N-acryloylglutamate) hydrogel.	254
S3.2 5. Shows the MALDI-TOF spectrum of p(NAG-Ac-NAE) hydrogel	255
S3.2 6. Biodegradation behavior of [p(NAG-Ac-NAE)] without replacing media, studied in PBS (pH 7.4) and in presence of different enzymes.	255
S3.2 7. (a) Size distribution and (b) zeta potential of p(NAG-Ac-NAE) hydrogel, studied in PBS (pH 7.4)	256
S3.2 8. (a) Cell viability of HUVEC cells in treatment of p(NAG-b-A) hydrogel, (b-e) Anti-angiogenic property of p(NAG-b-A) hydrogel. (a) Vessel area (%) vs Time, (b) Total number of junctions (%) vs Time, (c) Junction density (%) vs time and (d) Total Vessel length (%) vs time.	257

S3.3. 1. Docking poses for complex of GA9, GA15 and GA14	259
S3.3. 2. wound scratch assay on L929 cell line after treatment with p(Nag-co-Ac) hydrogel	259
S3.3. 3. Heparanase gene expression in cancer obtained from Human Protein Atlas	260
S3.3. 4. Heparanase gene expression in brain cancer and in breast cancer obtained from Human Protein Atlas	260

## LIST OF TABLES

---

<i>Table 1 Natural polymers used in neural tissue engineering,</i>	18
<i>Table 2 Polymer used for the angiogenesis and neurogenesis</i>	19
<i>Table 3 Clinically approved siRNA therapeutics</i>	29
<i>Table 4 Polymeric nanosystems for delivery of siRNA/ peptide and Drugs</i>	31
<i>Table S3.1. 1 Molecular interaction between GSK3<math>\beta</math> and reference inhibitor</i>	248
<i>Table S3.1. 2 Molecular interaction of GSK3<math>\beta</math> (Glycogen synthase kinase-3) with polymeric units</i>	248
<i>Table S3.2.1. Bioactivity of random structure of p(NAG-Ac-NAE) obtained through Molinspiration software</i>	257
<i>Table S3.3. 1. Bioactivity score of (a) homopolymer of n-acryloyl glycine (b) Linear hetro- polymer of n-acryloylglycine and acrylamide and (c) cross-linked homopolymer and (d) cross-linked hetropolymer represent p(NAG-co-Ac) polymer.</i>	261
<i>Table S3.3. 2. DFT calculation for (a) homopolymer of n-acryloyl glycine (b) Linear hetro- polymer of n-acryloyl glycine and acrylamide and (c) cross-linked homopolymer and (d) cross-linked hetropolymer represent p(NAG-co-Ac) polymer, changes in dipole moment and Intramolecular hydrogen bonding in different solvent</i>	263
<i>Table S3.3. 3 HOMO LUMO energy difference with increase in size of monomer to polymer and in presence of cross linker</i>	267
<i>Table S3.3.4: protein ligand interaction with heparanase PDBID-7PRT</i>	268